Inorganic Chemistry

Article

pubs.acs.org/IC

Manganese-Substituted Rare-Earth Zinc Arsenides $RE_{1-y}Mn_xZn_{2-x}As_2$ (*RE* = Eu−Lu) and $RE_{2-y}Mn_xZn_{4-x}As_4$ (*RE* = La−Nd, Sm, Gd)

Xinsong Lin, Danisa Tabassum, Brent W. Rudyk, and Arthur Mar*

Department of Chemistry, University of Alberta, Edmonton, Alberta Canada T6G 2G2

Supporting Information

ABSTRACT: Two series of Mn-substituted rare-earth zinc arsenides $RE_{1-y}Mn_xZn_{2-x}As_2$ (*RE* = Eu−Lu) and $RE_{2-y}Mn_xZn_{4-x}As_4$ (*RE* = La−Nd, Sm, Gd) were prepared by reaction of the elements at 750 °C. Both series are derived from ideal empirical formula REM_2As_2 (M = Mn, Zn) and adopt crystal structures related to the trigonal $CaAl_2Si_2$-type (space group $P\bar{3}m1$) in which hexagonal nets of *RE* atoms and $[M_2As_2]$ slabs built up of edge-sharing M-centered tetrahedra are alternately stacked along the *c*-direction. For compounds with divalent *RE* components (Eu, Yb), the fully stoichiometric and charge-balanced formula REM_2As_2 is obtained, with Mn and Zn atoms statistically disordered within the same tetrahedral site. For compounds with trivalent *RE* components, the *RE* sites become deficient, and the Mn atoms are segregated from the Zn atoms in separate tetrahedral sites. Within the series $RE_{1-y}Mn_xZn_{2-x}As_2$ (Gd−Tm, Lu), the parent $CaAl_2Si_2$-type structure is retained, and the Mn atoms are disordered within partially occupied interstitial sites above and below $[Zn_{2-x}As_2]$ slabs. Within the series $RE_{2-y}Mn_xZn_{4-x}As_4$ (*RE* = La−Nd, Sm, Gd), the *c*-axis becomes doubled as a result of partial ordering of Mn atoms between every other pair of $[Zn_{2-x}As_2]$ slabs. Attempts to synthesize Gd-containing solid solutions with the charge-balanced formula $Gd_{0.67}Mn_xZn_{2-x}As_2$ suggested that these phases could be formed with up to 50% Mn substitution. Band structure calculations reveal that a hypothetical superstructure model with the formula $La_{1.33}MnZn_3As_4$ would have no gap at the Fermi level and that slightly lowering the electron count alleviates antibonding Mn−As interactions; a spin-polarized calculation predicts nearly ferromagnetic half-metallic behavior. X-ray photoelectron spectroscopy confirms the presence of divalent Mn in these compounds.

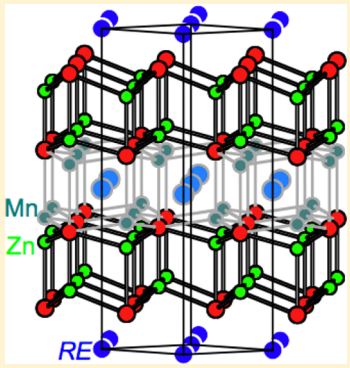

INTRODUCTION

Many ternary pnictides of the form AB_2X_2 adopt either the tetragonal $ThCr_2Si_2$-type ($I4/mmm$) or the trigonal $CaAl_2Si_2$-type ($P\bar{3}m1$) structure. The $ThCr_2Si_2$-type phases form for a wide variety of *B* components[1−3] and have long been renowned for their diverse physical properties, such as superconductivity in $BaFe_2As_2$-based materials.[4−7] The $CaAl_2Si_2$-type phases form for a more restricted set of *B* components[2,8−14] and have been identified as possible candidates for thermoelectric materials.[15−21] In both cases, doping is an important strategy for optimizing and improving properties; for example, superconductivity is induced in $BaFe_2As_2$ through hole doping (in $K_xBa_{1-x}Fe_2As_2$),[4] and thermoelectric transport properties can be tuned in $YbZn_2Sb_2$ through isovalent doping (in $Ca_xYb_{1-x}Zn_2Sb_2$).[22] Because subtle structural changes can often take place in the course of these chemical modifications, "substitution" is perhaps a more appropriate term than "doping."

It is desirable to extend the versatility of AB_2X_2 phases with the $CaAl_2Si_2$-type structure among ternary pnictides and to identify other potential applications of this class of compounds. All $CaAl_2Si_2$-type phases known so far appear to conform quite strictly to the requirement of d^0, d^5, or d^{10} configurations for the *B* component.[2,8−10] There is also a weaker condition of an ideal valence electron count of 16 e^-/f.u., corresponding to a charge-balanced formulation and, in principle, the presence of a small band gap between filled valence and empty conduction bands, leading to the semiconducting behavior required in thermoelectric materials. This electron count is occasionally violated, as in $REAl_2Si_2$ and $REAl_2Ge_2$ (17 e^-/f.u.), because the expected band gap has vanished; semimetallic behavior develops instead.[11,12] Ternary pnictides satisfying both conditions are well-known for AM_2Pn_2 (*A* = alkaline-earth or divalent rare-earth metal; M = Mg, Mn, Zn, Cd; Pn = P, As, Sb, Bi).[23] These can be extended to phases containing rare-earth metals as the *A* component, while maintaining the electron count, through formation of defects in ternary arsenides $RE_{0.67}Zn_2As_2$[24] or through aliovalent substitution with two different metals as the *B* component in quaternary pnictides $REMM'Pn_2$ (M = Ag, Cu; M′ = Mn, Zn; Pn = P, As, Sb).[25−33] Through these investigations, there is now greater understanding of the influence of the chemical substituents on the size of the band gap. For example, judicious combinations of M and M′ components (such as Cu−Zn) may narrow the band gap so that the valence and conduction bands just touch.[33] In this way, solid solutions $GdCu_xZn_{2-x}P_2$ ($1.0 \le x \le 1.3$) are formed in which the electron count can deviate from 16 e^-/f.u.[31] Similar types of

Received: May 5, 2014
Published: July 25, 2014

   dx.doi.org/10.1021/ic501053v | *Inorg. Chem.* 2014, 53, 8431−8441

limited solid solutions have been found in the related silicides $GdMn_xAl_{2-x}Si_2$ ($0 \le x \le 0.25$) and germanides $GdZn_xAl_{2-x}Ge_2$ ($0 \le x \le 1.0$).[11,12] Efforts are now underway to evaluate thermoelectric properties tuned through appropriate substitution in solid solutions of various phosphides $(Ca/Yb)(Mn/Cu/Zn)_2P_2$[34,35] and antimonides $(Ca/Eu/Yb)(Mn/Zn/Cd)_2Sb_2$.[22,36−41] The presence of two-dimensional slabs in $CaAl_2Si_2$-type phases conforms with the realization that simple layered structures with anisotropic bonding may be favorable for exhibiting the low thermal conductivity required for good thermoelectric performance.[42] Substitution with Mn may impart interesting magnetic properties, although these have not yet been investigated in detail. It is worth noting, however, that $Li_{1+y}Mn_xZn_{1-x}Pn$ (Pn = P, As) have recently been touted as "new-generation" dilute ferromagnetic semiconductors;[43,44] they adopt a filled zincblende-type structure, from which the $CaAl_2Si_2$-type structure can be derived.

We have been systematically investigating the ternary rare-earth zinc arsenide systems *RE*−Zn−As, which contain not only $CaAl_2Si_2$-type phases ($REZn_2As_2$ (*RE* = Eu, Yb) and $RE_{0.67}Zn_2As_2$ (*RE* = La−Nd, Sm)),[24,27,28,45−48] but also many other phases with diverse structures ($REZn_2As_3$ (*RE* = La−Pr); $REZn_{0.67}As_2$, $REZn_3As_3$, $REZn_{2-x}As_2{\cdot}n(REAs)$ (n = 3, 4, 5, 6) for *RE* = La−Nd, Sm; $Eu_2Zn_2As_3$, $Eu_{11}Zn_6As_{12}$).[49−54] Manganese substitution appears to be viable in these systems, as suggested by the formation of the two compounds $Ce_4(Mn,Zn)_{2-x}As_5$ and $Ce_6(Mn,Zn)_{2-x}As_7$ within the homologous series $REZn_{2-x}As_2{\cdot}n(REAs)$, which is derived from the intergrowth of $CaAl_2Si_2$-type slabs with rock salt-type slabs [*RE*As] of variable thickness.[52] Herein we report the preparation of quaternary arsenides in which the partial substitution of Mn for Zn leads to two distinct series forming for the earlier ($RE_{2-y}Mn_xZn_{4-x}As_4$; *RE* = La−Nd, Sm, Gd) versus later rare-earth members ($RE_{1-y}Mn_xZn_{2-x}As_2$; *RE* = Eu−Lu). The $RE_{1-y}Mn_xZn_{2-x}As_2$ series is closely related to the parent *RE*-defective arsenides $RE_{0.67}Zn_2As_2$, but the $RE_{2-y}Mn_xZn_{4-x}As_4$ series has a doubled trigonal *c*-parameter. The structural effects of Mn substitution are more complicated than anticipated and are explored within the series $Gd_{0.67}Mn_xZn_{2-x}As_2$. Band structure calculations were carried out to examine how the band gap is influenced by this Mn substitution. X-ray photoelectron spectra (XPS) were collected to probe the valence state of the Mn atoms in these compounds.

EXPERIMENTAL SECTION

Synthesis. Starting materials were freshly filed *RE* pieces (99.9%, Hefa), Mn powder (99.99%, Aldrich), Zn shot (99.99%, Aldrich), and As lumps (99.999%, Alfa-Aesar). These elements were initially combined on a 0.3-g scale with the loading composition of $RE_{0.67}MnZnAs_2$ to target the preparation of defective $CaAl_2Si_2$-type phases for various *RE* components. Subsequent energy-dispersive X-ray (EDX) analysis suggested slightly different compositions than those loaded for some crystals resulting from the syntheses, corresponding to approximately 10% *RE*, 10% Mn, 40% Zn, and 40% As. Ultimately, the *RE*/Mn/Zn/As ratios used in obtaining the title compounds were 0.67:1:1:2 for the $RE_{1-y}Mn_xZn_{2-x}As_2$ (*RE* = Eu−Lu) series and 1:1:4:4 for the $RE_{2-y}Mn_xZn_{4-x}As_4$ (*RE* = La−Nd, Sm, Gd) series. The mixtures were loaded into fused-silica tubes, which were evacuated and sealed. The tubes were heated at 500 °C for 2 d, heated to 750 °C over 20 h, held at this temperature for 7 d, and then cooled to room temperature over 10 h. The preheating step at 500 °C was included to minimize loss of the volatile components (Zn and As). Powder X-ray diffraction (XRD) patterns were collected on an Inel powder diffractometer equipped with a curved position-sensitive detector (CPS 120) and a Cu Kα_1 radiation source operated at 40 kV and 20 mA. The products consisted of the title compounds as the major phases, with binary arsenides and small amounts of other ternary arsenides as minor phases, as shown in representative powder XRD patterns (Figures S1 and S2 in Supporting Information). Phase relationships in arsenide systems remain poorly understood, and further work is in progress to elucidate them. To promote the growth of crystals suitable for structure determination, the as-prepared samples were reheated at 800 °C for 2 d, heated to 1050 °C over 20 h, held at this temperature for 7 d, slowly cooled to 500 °C at a rate of 3 °C/h, and then cooled to room temperature over 2 d. Crystals tended to grow as thinner plates in the $RE_{2-y}Mn_xZn_{4-x}As_4$ (*RE* = La−Nd, Sm, Gd) series than in the $RE_{1-y}Mn_xZn_{2-x}As_2$ (*RE* = Eu−Lu) series. Crystals obtained from these reactions were examined by EDX analysis on a JEOL JSM-6010LA scanning electron microscope. Mn is distributed uniformly within these crystals, as seen in elemental maps for a representative sample (Figure S3 in Supporting Information). These analyses generally agree with the expected chemical compositions based on the formulas deduced from the single-crystal structure determinations below (Table S1 in Supporting Information). However, the observed Mn content in some of the $RE_{1-y}Mn_xZn_{2-x}As_2$ members was somewhat larger than the expected value of 9 atom % based on the average formula of $RE_{0.5}Mn_{0.4}Zn_{1.6}As_2$. This discrepancy can be attributed to systematic errors in the EDX analysis caused by partial peak overlap of Mn K and *RE* L lines for some of these compounds; it may also reflect an actual variation in composition depending on the *RE* member or inaccuracies in occupancy refinements in the structure determinations.

Structure Determination. Intensity data were collected at room temperature on a Bruker PLATFORM diffractometer equipped with a SMART APEX II CCD area detector and a graphite-monochromated Mo Kα radiation source, using ω scans in 5−8 batches at different ϕ angles with a frame width of 0.3° and an exposure time of 12−20 s per frame. Face-indexed absorption corrections were applied. Structure solution and refinement were carried out with use of the SHELXTL (version 6.12) program package.[55]

For the series of $RE_{1-y}Mn_xZn_{2-x}As_2$ (*RE* = Eu−Lu), the unit cell parameters ($a \approx 4$ Å, $c \approx 7$ Å) and the intensity symmetry were consistent with the centrosymmetric trigonal space group $P\bar{3}m1$ adopted by the expected $CaAl_2Si_2$-type structure.[56] For the divalent *RE* members of this series (*RE* = Eu, Yb), direct methods revealed the locations of the three sites within this structure: 1*a* (0, 0, 0) occupied by *RE* atoms, 2*d* (1/3, 2/3, ∼0.63) occupied by a statistical mixture of Mn and Zn atoms, and 2*d* (1/3, 2/3, ∼0.26) occupied by As atoms. When the occupancies of the transition-metal site were allowed to vary, with the constraint that they sum to unity, they converged to 0.22(2) Mn/0.78(2) Zn in the Eu member and 0.16(3) Mn/0.84(3) Zn in the Yb member. The *RE* and As sites were found to be fully occupied, although a slight Yb substoichiometry of 0.95(1) was found in the Yb member. The resulting formulas, $EuMn_{0.4}Zn_{1.6}As_2$ and $YbMn_{0.3}Zn_{1.7}As_2$, are electron-precise or very nearly so, with the assumption that Mn and Zn atoms are divalent. For the trivalent *RE* members of this series (*RE* = Gd−Tm, Lu), refinement of similar models based on the $CaAl_2Si_2$-type structure led to elevated displacement parameters for the *RE* sites ($U_{eq} \approx 0.03$ Å^2), implying that they are partially occupied. When freed, the occupancies of the *RE* sites converged to 0.51−0.53 for most members (*RE* = Gd−Er) but to slightly lower values of 0.42−0.43 for two later ones (*RE* = Tm, Lu). Inspection of the difference Fourier maps revealed residual electron density at 2*d* (1/3, 2/3, ∼0.82), typically ∼10 e$^-$/Å^3, that is close to the original transition-metal site at 2*d* (1/3, 2/3, ∼0.63). Because these two sites are within ∼1.3 Å from each other, they were each allowed to contain a disordered mixture of Mn and Zn atoms, with the constraint that the total occupancy over both sites sum to unity. In general, these refinements led to occupancy ranges from 0.0(1) to 0.1(1) Mn and from 0.7(1) to 0.8(1) Zn in the site at 1/3, 2/3, ∼0.63, in contrast to ranges from 0.0(1) to 0.3(1) Mn and from −0.1(1) to 0.1(1) Zn in the site at 1/3, 2/3, ∼0.82. That is, there is a primary site that is clearly preferred by Zn atoms and a secondary site that shows a slight preference for Mn atoms. To treat subsequent refinements on a consistent basis, we applied a simplified structural model containing only Zn atoms in the primary site and Mn atoms in the secondary site,

dx.doi.org/10.1021/ic501053v | Inorg. Chem. 2014, 53, 8431−8441

constrained such that their occupancies sum to unity, while the *RE* site was allowed to be partially occupied. The resulting formulas, generally $RE_{0.5}Mn_{0.4}Zn_{1.6}As_2$ for most members, suggest slightly more pronounced *RE* deficiencies relative to the electron-precise ones assumed for the related ternary arsenides $RE_{0.67}Zn_2As_2$. As a test of the consistency of this refinement procedure, two data sets for separate crystals of the Gd-containing member obtained from the same reaction batch were collected. The resulting formulas from the structure refinements on these crystals were $Gd_{0.52(1)}Mn_{0.40(1)}Zn_{1.60(1)}As_2$ and $Gd_{0.51(1)}Mn_{0.43(2)}Zn_{1.57(2)}As_2$, in good agreement with each other.

For the series $RE_{2-y}Mn_xZn_{4-x}As_4$ (*RE* = La–Nd, Sm, Gd), the intensity symmetry also suggested the trigonal space group $P\bar{3}m1$, but there is a doubling in the unit cell *c*-parameter to ~14 Å. This doubling can be clearly seen in a comparison of the 0*kl* nets for crystals of $Gd_{1-y}Mn_xZn_{2-x}As_2$ versus $Gd_{2-y}Mn_xZn_{4-x}As_4$, which was found to occur in both possible forms (Figure 1). Direct methods provided a

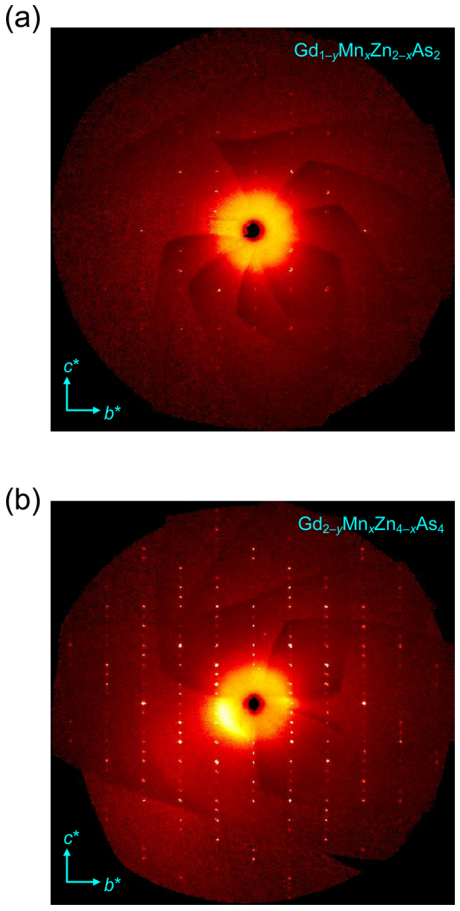

Figure 1. 0*kl* nets for crystals of (a) $Gd_{1-y}Mn_xZn_{2-x}As_2$ and (b) $Gd_{2-y}Mn_xZn_{4-x}As_4$.

model corresponding to a superstructure of the $CaAl_2Si_2$-type (with two *RE*, two transition-metal, and two As sites). Refinement of this model indicated full occupancy for the *RE* site at 1*a* (0, 0, 0) but partial occupancy of ~0.2–0.3 for the *RE* site at 1*b* (0, 0, 1/2). Inspection of difference Fourier maps revealed residual electron density corresponding to a third transition-metal site close to (within ~1.2 Å) an existing one. Each of these sites was allowed to be occupied by a mixture of Mn and Zn atoms, with the constraint that the occupancies of the two closely spaced ones (at 1/3, 2/3, ~0.33 and 1/3, 2/3, ~0.41) sum to unity. These refinements led to occupancies of 0.0(2) Mn/0.6(2) Zn (at 1/3, 2/3, ~0.33), 0.2(2) Mn/0.2(2) Zn (at 1/3, 2/3, ~0.41), and 0.1(1) Mn/0.9(1) Zn (at 1/3, 2/3, ~0.80). Again, to simplify the structural analysis, we applied an ordered model in which Mn atoms exclusively occupy the site at 1/3, 2/3, ~0.41, and Zn atoms occupy the other two sites. For most members, subsequent refinements gave resulting formulas of $RE_{1.3}Mn_{0.9}Zn_{3.1}As_4$, essentially in agreement with expectations according to charge balance. For a couple of the structures, such as the Nd-containing member, this simplification leads to slightly worse agreement factors and slightly higher residual electron density in the difference map; however, for ease of comparison, we prefer to retain this ordered structural model for all members.

Atomic positions were standardized with the program STRUCTURE TIDY.[57] The compounds $RE_{1-y}Mn_xZn_{2-x}As_2$ (*RE* = Gd–Tm, Lu) contain an extra transition-metal site relative to the $CaAl_2Si_2$-type structure; because this standardization changes the choice of equivalent positions, we opted to retain coordinates to match with the parent structure in these cases. Abbreviated crystallographic data are summarized in Tables 1 and 2, positional and displacement parameters are listed in Tables 3 and 4, and selected interatomic distances are listed in Tables 5 and 6. Full crystallographic details are listed in Tables S2 and S3 in Supporting Information. Further data, in the form of crystallographic information files (CIFs), are available as Supporting Information.

Band Structure Calculation. Tight-binding linear muffin tin orbital band structure calculations were performed within the local density and atomic spheres approximation with use of the Stuttgart TB-LMTO-ASA program (version 4.7).[58] With cell parameters and atomic coordinates taken from the experimental crystal structure of $La_{1.3}Mn_{0.9}Zn_{3.1}As_4$, an idealized model $La_{1.33}MnZn_3As_4$ was considered, based on a hypothetical $\sqrt{3}a \times \sqrt{3}a$ superstructure in the lower-symmetry space group $P31m$ (No. 157) and an ordered distribution of the partially occupied La1 (33%), Mn (50%), and Zn1 (50%) sites. The basis set consisted of La 6s/6p/5d/4f, Mn 4s/4p/3d, Zn 4s/4p/3d, and As 4s/4p orbitals, with the La 6p and As 4d orbitals being downfolded. Integrations in reciprocal space were carried out with an improved tetrahedron method over 384 irreducible *k*-points with the first Brillouin zone. The calculations were performed initially without spin polarization and then repeated with spin polarization included.

XPS Analysis. $YbMn_{0.3}Zn_{1.7}As_2$, $Er_{0.5}Mn_{0.4}Zn_{1.6}As_2$, and $Nd_{1.2}Mn_{1.0}Zn_{3.0}As_4$ were chosen as representative samples to be examined by XPS. Yb_2O_3 was also measured as a standard sample containing trivalent Yb. XPS spectra were collected on a Kratos AXIS Ultra spectrometer equipped with a monochromatic Al Kα X-ray source (operated at 12 mA and 12 kV) and a hybrid lens (with spot size of 700 μm × 400 μm). The samples were finely ground, pressed into pellets (6 mm diameter, 1–3 mm thickness), and secured onto a sample bar with double-sided tape. The samples were transferred via a load-lock into the analysis chamber, which was held at a pressure between 10^{-7} and 10^{-9} Pa. The samples were sputter-cleaned with an Ar^+-ion beam (4 kV, 10 mA) until the intensity of the O 1s peak remained constant, indicating that no further surface oxides could be removed. Yb_2O_3, $Er_{0.5}Mn_{0.4}Zn_{1.6}As_2$, and $Nd_{1.2}Mn_{1.0}Zn_{3.0}As_4$ were each sputtered for 5 min, whereas $YbMn_{0.3}Zn_{1.7}As_2$ required an additional 5 min of sputtering to reduce background noise levels. The presence of a shoulder in the Mn 2p spectra indicated that slight reduction occurred as a result of this Ar^+ sputtering procedure. Survey spectra were collected with pass energy of 80 eV, step size of 0.4 eV, and dwell time of 0.1 s over the range of 1100 to 0 eV. They confirmed the presence of all expected elements. High-resolution Yb 4d and Mn 2p spectra were collected with pass energy of 20 eV, step size of 0.1 eV, and dwell time of 0.2 s over ranges determined from the survey spectra. These spectra were calibrated to the C 1s peak located at 284.8 eV arising from adventitious carbon. Because the Mn 2p signal for $YbMn_{0.3}Zn_{1.7}As_2$ was found to be weaker than the others, this spectrum was collected with a step size of 0.05 eV. All spectra were analyzed with use of the CasaXPS software package.[59] The background was removed through a Shirley function, and the peaks were fitted to pseudo-Voigt (70% Gaussian and 30% Lorentzian) profiles to account for instrumental and experimental broadening effects. The uncertainty of this spectrometer is generally estimated as better than ±0.1 eV on the basis of previous measurements, but this must be counterbalanced by the relatively low concentration of Mn in these samples. Charge neutralization was required only for the Yb_2O_3 standard and was applied to maximize signal intensity and minimize peak widths.

dx.doi.org/10.1021/ic501053v | Inorg. Chem. 2014, 53, 8431–8441

Table 1. Crystallographic Data for $RE_{1-y}Mn_xZn_{2-x}As_2$ (RE = Eu−Lu)[a]

formula	fw (amu)	a (Å)	c (Å)	V (Å^3)	ρ_c (g cm^{-3})	μ (mm^{-1})	$R(F)$[b]	$R_w(F_o^2)$[c]
$EuMn_{0.44(6)}Zn_{1.56(6)}As_2$	427.95	4.234(2)	7.198(4)	111.74(14)	6.360	37.86	0.026	0.043
$Gd_{0.52(1)}Mn_{0.40(1)}Zn_{1.60(1)}As_2$	355.03	4.109(3)	6.703(5)	98.02(13)	6.014	35.88	0.034	0.060
$Tb_{0.52(1)}Mn_{0.42(1)}Zn_{1.58(1)}As_2$	355.87	4.1135(4)	6.7246(7)	98.54(2)	5.997	36.25	0.025	0.050
$Dy_{0.53(1)}Mn_{0.42(1)}Zn_{1.58(1)}As_2$	362.32	4.1023(9)	6.7197(16)	97.93(4)	6.143	37.49	0.031	0.062
$Ho_{0.53(1)}Mn_{0.39(1)}Zn_{1.61(1)}As_2$	363.93	4.091(3)	6.700(11)	97.1(2)	6.223	38.50	0.032	0.072
$Er_{0.51(1)}Mn_{0.38(1)}Zn_{1.62(1)}As_2$	360.04	4.103(5)	6.722(7)	98.02(19)	6.099	38.13	0.031	0.045
$Tm_{0.43(1)}Mn_{0.21(1)}Zn_{1.79(1)}As_2$	351.03	4.0980(18)	6.664(3)	96.91(7)	6.015	38.16	0.021	0.045
$Yb_{0.95(1)}Mn_{0.32(6)}Zn_{1.68(6)}As_2$	441.84	4.1682(6)	6.9478(10)	104.54(3)	7.018	47.12	0.018	0.040
$Lu_{0.42(1)}Mn_{0.20(1)}Zn_{1.80(1)}As_2$	348.48	4.0932(9)	6.6433(14)	96.39(4)	6.003	38.75	0.021	0.050

[a]For all structures, Z = 1, T = 296(2) K, λ = 0.710 73 Å, space group $P\bar{3}m1$ (No. 164). [b]$R(F) = \sum||F_o| - |F_c||/\sum|F_o|$ for $F_o^2 > 2\sigma(F_o^2)$. [c]$R_w(F_o^2) = [\sum[w(F_o^2 - F_c^2)^2]/\sum wF_o^4]^{1/2}$; $w^{-1} = [\sigma^2(F_o^2) + (Ap)^2 + Bp]$, where $p = [\max(F_o^2,0) + 2F_c^2]/3$.

Table 2. Crystallographic Data for $RE_{2-y}Mn_xZn_{4-x}As_4$ (RE = La−Nd, Sm, Gd)[a]

formula	fw (amu)	a (Å)	c (Å)	V (Å^3)	ρ_c (g cm^{-3})	μ (mm^{-1})	$R(F)$[b]	$R_w(F_o^2)$[c]
$La_{1.25(1)}Mn_{0.93(2)}Zn_{3.07(2)}As_4$	722.33	4.159(2)	13.639(7)	204.3(2)	5.870	32.53	0.052	0.113
$Ce_{1.30(1)}Mn_{0.83(3)}Zn_{3.17(3)}As_4$	734.66	4.156(5)	13.569(16)	203.0(5)	6.010	33.69	0.044	0.125
$Pr_{1.25(1)}Mn_{0.95(2)}Zn_{3.05(2)}As_4$	727.39	4.1533(4)	13.5629(13)	202.61(4)	5.961	33.81	0.033	0.097
$Nd_{1.25(1)}Mn_{0.95(3)}Zn_{3.05(3)}As_4$	731.55	4.1283(17)	13.513(6)	199.45(14)	6.091	34.84	0.067	0.144
$Sm_{1.24(1)}Mn_{0.87(4)}Zn_{3.13(4)}As_4$	738.52	4.1240(19)	13.507(6)	198.9(2)	6.164	36.04	0.051	0.153
$Gd_{1.24(1)}Mn_{0.93(3)}Zn_{3.07(3)}As_4$	746.45	4.1180(14)	13.500(5)	198.27(15)	6.252	37.27	0.048	0.135

[a]For all structures, Z = 1, T = 296(2) K, λ = 0.710 73 Å, space group $P\bar{3}m1$ (No. 164). [b]$R(F) = \sum||F_o| - |F_c||/\sum|F_o|$ for $F_o^2 > 2\sigma(F_o^2)$. [c]$R_w(F_o^2) = [\sum[w(F_o^2 - F_c^2)^2]/\sum wF_o^4]^{1/2}$; $w^{-1} = [\sigma^2(F_o^2) + (Ap)^2 + Bp]$, where $p = [\max(F_o^2,0) + 2F_c^2]/3$.

Table 3. Atomic Coordinates and Equivalent Isotropic Displacement Parameters (Å^2)[a] for $RE_{1-y}Mn_xZn_{2-x}As_2$ (RE = Eu−Lu)

	$EuMn_{0.44(6)}Zn_{1.56(6)}As_2$	$Gd_{0.52(1)}Mn_{0.40(1)}Zn_{1.60(1)}As_2$	$Tb_{0.52(1)}Mn_{0.42(1)}Zn_{1.58(1)}As_2$	$Dy_{0.53(1)}Mn_{0.42(1)}Zn_{1.58(1)}As_2$	$Ho_{0.53(1)}Mn_{0.39(1)}Zn_{1.61(1)}As_2$
RE in 1a (0, 0, 0)					
occupancy	1	0.517(4)	0.516(4)	0.526(4)	0.526(4)
U_{eq}	0.0123(3)	0.0164(5)	0.0167(3)	0.0192(4)	0.0223(5)
Mn in 2d (1/3, 2/3, z)					
occupancy	0.22(3)	0.195(6)	0.209(5)	0.210(6)	0.194(6)
z	0.6283(2)	0.825(2)	0.816(2)	0.818(3)	0.818(3)
U_{eq}	0.0138(5)	0.042(4)	0.058(4)	0.052(5)	0.053(5)
Zn in 2d (1/3, 2/3, z)					
occupancy	0.78(3)	0.805(6)	0.791(5)	0.790(6)	0.806(6)
z	0.6283(2)	0.6262(3)	0.6259(2)	0.6262(3)	0.6269(3)
U_{eq}	0.0138(5)	0.0214(6)	0.0225(4)	0.0250(6)	0.0258(6)
As in 2d (1/3, 2/3, z)					
z	0.26553(15)	0.24252(18)	0.24267(12)	0.24278(16)	0.24212(17)
U_{eq}	0.0105(3)	0.0141(4)	0.0137(3)	0.0160(3)	0.0181(4)

	$Er_{0.51(1)}Mn_{0.38(1)}Zn_{1.62(1)}As_2$	$Tm_{0.43(1)}Mn_{0.21(1)}Zn_{1.79(1)}As_2$	$Yb_{0.95(1)}Mn_{0.32(6)}Zn_{1.68(6)}As_2$	$Lu_{0.42(1)}Mn_{0.20(1)}Zn_{1.80(1)}As_2$
RE in 1a (0, 0, 0)				
occupancy	0.511(3)	0.434(3)	0.945(4)	0.419(3)
U_{eq}	0.0203(4)	0.0207(4)	0.01103(18)	0.0213(3)
Mn in 2d (1/3, 2/3, z)				
occupancy	0.190(5)	0.105(5)	0.16(3)	0.098(4)
z	0.821(2)	0.830(4)	0.63102(15)	0.836(6)
U_{eq}	0.052(5)	0.068(8)	0.0122(3)	0.076(9)
Zn in 2d (1/3, 2/3, z)				
occupancy	0.810(5)	0.895(5)	0.84(3)	0.902(4)
z	0.6274(3)	0.62910(16)	0.63102(15)	0.62957(16)
U_{eq}	0.0244(5)	0.0195(3)	0.0122(3)	0.0202(3)
As in 2d (1/3, 2/3, z)				
z	0.24177(15)	0.23759(10)	0.25508(11)	0.23669(10)
U_{eq}	0.0168(3)	0.0137(2)	0.0094(3)	0.0139(2)

[a]U_{eq} is defined as one-third of the trace of the orthogonalized U_{ij} tensor.

RESULTS AND DISCUSSION

Within ternary RE−Zn−As systems, $CaAl_2Si_2$-type phases were previously restricted to $REZn_2As_2$ (RE = Eu, Yb), containing divalent RE components only.[27,28,45−48] They have been recently extended to $RE_{0.67}Zn_2As_2$ (RE = La−Nd, Sm), containing early trivalent RE components but with formation of

dx.doi.org/10.1021/ic501053v | Inorg. Chem. 2014, 53, 8431−8441

Table 4. Atomic Coordinates and Equivalent Isotropic Displacement Parameters (Å^2)[a] for $RE_{2-y}Mn_xZn_{4-x}As_4$ (RE = La−Nd, Sm, Gd)

	$La_{1.25(1)}Mn_{0.93(2)}Zn_{3.07(2)}As_4$	$Ce_{1.30(1)}Mn_{0.83(3)}Zn_{3.17(3)}As_4$	$Pr_{1.25(1)}Mn_{0.95(2)}Zn_{3.05(2)}As_4$	$Nd_{1.25(1)}Mn_{0.95(3)}Zn_{3.05(3)}As_4$	$Sm_{1.24(1)}Mn_{0.87(4)}Zn_{3.13(4)}As_4$	$Gd_{1.24(1)}Mn_{0.93(3)}Zn_{3.07(3)}As_4$
*RE*1 in 1*b* (0, 0, 1/2)						
occupancy	0.246(10)	0.300(10)	0.253(8)	0.249(14)	0.240(10)	0.242(9)
U_{eq}	0.039(3)	0.036(2)	0.035(2)	0.044(5)	0.031(3)	0.033(3)
*RE*2 in 1*a* (0, 0, 0)						
occupancy	1	1	1	1	1	1
U_{eq}	0.0165(4)	0.0185(4)	0.0147(3)	0.0132(5)	0.0226(6)	0.0166(4)
Mn in 2*d* (1/3, 2/3, *z*)						
occupancy	0.466(12)	0.414(13)	0.477(10)	0.476(17)	0.436(18)	0.468(15)
z	0.4095(8)	0.4099(10)	0.4087(7)	0.4097(12)	0.4086(14)	0.4079(11)
U_{eq}	0.034(3)	0.037(3)	0.038(2)	0.031(4)	0.034(4)	0.034(3)
Zn1 in 2*d* (1/3, 2/3, *z*)						
occupancy	0.534(12)	0.586(13)	0.523(10)	0.524(17)	0.564(18)	0.533(15)
z	0.3364(4)	0.3324(4)	0.3331(3)	0.3339(7)	0.3324(7)	0.3318(6)
U_{eq}	0.0230(16)	0.0225(15)	0.0215(11)	0.020(2)	0.024(2)	0.0220(18)
Zn2 in 2*d* (1/3, 2/3, *z*)						
occupancy	1	1	1	1	1	1
z	0.79987(16)	0.80160(18)	0.80174(13)	0.8020(2)	0.8035(2)	0.8037(2)
U_{eq}	0.0186(5)	0.0174(6)	0.0169(4)	0.0157(7)	0.0196(8)	0.0186(6)
As1 in 2*d* (1/3, 2/3, *z*)						
z	0.13326(12)	0.13196(14)	0.13056(9)	0.12920(18)	0.12714(19)	0.12611(15)
U_{eq}	0.0125(4)	0.0114(4)	0.0100(3)	0.0091(5)	0.0132(6)	0.0105(4)
As2 in 2*d* (1/3, 2/3, *z*)						
z	0.61635(14)	0.61568(16)	0.61690(11)	0.6176(2)	0.6185(2)	0.61946(17)
U_{eq}	0.0180(4)	0.0162(5)	0.0162(3)	0.0153(6)	0.0186(6)	0.0177(5)

[a] U_{eq} is defined as one-third of the trace of the orthogonalized U_{ij} tensor.

Table 5. Interatomic Distances (Å) for $RE_{1-y}Mn_xZn_{2-x}As_2$ (RE = Eu−Lu)

	$EuMn_{0.4}Zn_{1.6}As_2$	$Gd_{0.5}Mn_{0.4}Zn_{1.6}As_2$	$Tb_{0.5}Mn_{0.4}Zn_{1.6}As_2$	$Dy_{0.5}Mn_{0.4}Zn_{1.6}As_2$	$Ho_{0.5}Mn_{0.4}Zn_{1.6}As_2$
RE−As (× 6)	3.103(1)	2.876(2)	2.882(1)	2.876(1)	2.865(2)
RE−Mn (× 6)	3.624(2)	2.647(7)	2.678(7)	2.667(8)	2.660(10)
Mn−As (× 3)	2.561(1)	2.415(3)	2.408(3)	2.403(3)	2.396(4)
Mn−As	2.612(2)	2.799(15)	2.869(16)	2.857(18)	2.84(2)
Zn−As (× 3)	2.561(1)	2.530(2)	2.534(1)	2.527(1)	2.520(2)
Zn−As	2.612(2)	2.572(3)	2.577(2)	2.576(2)	2.578(5)
Zn−Zn (× 3)	3.064(2)	2.914(3)	2.917(2)	2.913(2)	2.910(3)
	$Er_{0.5}Mn_{0.4}Zn_{1.6}As_2$	$Tm_{0.4}Mn_{0.2}Zn_{1.8}As_2$	$Yb_{1.0}Mn_{0.3}Zn_{1.7}As_2$	$Lu_{0.4}Mn_{0.2}Zn_{1.8}As_2$	
RE−As (× 6)	2.873(2)	2.847(1)	2.989(1)	2.838(1)	
RE−Mn (× 6)	2.658(7)	2.623(13)	3.516(1)	2.602(15)	
Mn−As (× 3)	2.406(4)	2.409(6)	2.533(1)	2.412(7)	
Mn−As	2.830(16)	2.72(3)	2.612(1)	2.66(4)	
Zn−As (× 3)	2.527(3)	2.527(1)	2.533(1)	2.525(1)	
Zn−As	2.592(3)	2.609(2)	2.612(1)	2.610(1)	
Zn−Zn (× 3)	2.924(3)	2.926(2)	3.018(1)	2.924(1)	

Table 6. Interatomic Distances (Å) for $RE_{2-y}Mn_xZn_{4-x}As_4$ (RE = La−Nd, Sm, Gd)

	$La_{1.2}Mn_{0.9}Zn_{3.1}As_4$	$Ce_{1.3}Mn_{0.8}Zn_{3.2}As_4$	$Pr_{1.2}Mn_{1.0}Zn_{3.0}As_4$	$Nd_{1.2}Mn_{1.0}Zn_{3.0}As_4$	$Sm_{1.2}Mn_{0.9}Zn_{3.1}As_4$	$Gd_{1.2}Mn_{0.9}Zn_{3.1}As_4$
*RE*1−As2 (× 6)	2.878(2)	2.867(3)	2.875(1)	2.864(2)	2.869(2)	2.873(2)
*RE*1−Mn (× 6)	2.700(5)	2.693(7)	2.698(4)	2.677(7)	2.682(9)	2.683(7)
*RE*2−As1 (× 6)	3.012(2)	2.994(3)	2.981(1)	2.955(2)	2.936(2)	2.924(1)
Mn−As2 (× 3)	2.427(2)	2.425(4)	2.423(1)	2.412(3)	2.409(3)	2.406(2)
Mn−As2	2.821(11)	2.792(14)	2.823(9)	2.808(16)	2.835(19)	2.856(14)
Zn1−As2 (× 3)	2.486(2)	2.501(3)	2.492(1)	2.472(3)	2.472(3)	2.467(2)
Zn1−As1	2.771(6)	2.719(7)	2.747(5)	2.766(9)	2.772(10)	2.777(8)
Zn2−As2	2.503(3)	2.523(4)	2.507(2)	2.493(4)	2.499(4)	2.488(3)
Zn2−As1 (× 3)	2.569(2)	2.563(3)	2.568(1)	2.558(2)	2.559(2)	2.559(1)
Zn1−Zn2 (× 3)	3.037(4)	3.010(5)	3.016(3)	3.009(6)	3.006(7)	3.000(5)

dx.doi.org/10.1021/ic501053v | Inorg. Chem. 2014, 53, 8431−8441

defects to satisfy the ideal electron count of 16 e^-/f.u.[24] We initially attempted to prepare the defective $RE_{0.67}Zn_2As_2$ phases containing later trivalent *RE* components (*RE* = Gd−Tm, Lu), using various synthetic conditions ranging from 750 to 1050 °C, but were unsuccessful. Given the existence of the Mn-containing counterparts $REMn_2As_2$ (*RE* = Eu, Yb),[60] we also attempted to prepare defective $RE_{0.67}Mn_2As_2$ phases containing various trivalent *RE* components, to no avail. Thus, it was surprising to discover that *partial* Mn substitution enables the preparation of two extensive series of quaternary arsenides, $RE_{1-y}Mn_xZn_{2-x}As_2$ (*RE* = Eu−Lu) and $RE_{2-y}Mn_xZn_{4-x}As_4$ (*RE* = La−Nd, Sm, Gd), for all possible *RE* components (except Pm, of course). The syntheses of these compounds are beset by difficulties posed by volatilization of Zn and As at high temperatures, so that the products normally contain admixtures of binary arsenides such as Zn_3As_2. However, slow cooling from 1050 to 500 °C was successful in the growth of single crystals to permit detailed structural analysis. Further optimization of synthetic conditions is in progress to improve the phase purity of these samples.

Individual *RE* members from these series were characterized by single-crystal structure determinations. The average compositions obtained from structure refinements were $REMn_{0.4}Zn_{1.6}As_2$ (*RE* = Eu, Yb), $RE_{0.5}Mn_{0.4}Zn_{1.6}As_2$ (*RE* = Gd−Tm, Lu), and $RE_{1.3}Mn_{0.9}Zn_{3.1}As_4$ (*RE* = La−Nd, Sm, Gd). For concreteness and simplicity, we use these average formulas in subsequent discussion when referring to these sets of compounds. They crystallize in the trigonal space group $P\bar{3}m1$, but the *c*-axis is doubled in $RE_{1.3}Mn_{0.9}Zn_{3.1}As_4$, which can be regarded as a superstructure of $RE_{0.5}Mn_{0.4}Zn_{1.6}As_2$. A plot of the cell parameters (with *c*-axis and cell volume *V* halved in $RE_{1.3}Mn_{0.9}Zn_{3.1}As_4$ for comparison to the subcell) illustrates the expected lanthanide contraction, but with deviations observed for members containing the larger divalent Eu and Yb components (Figure 2).

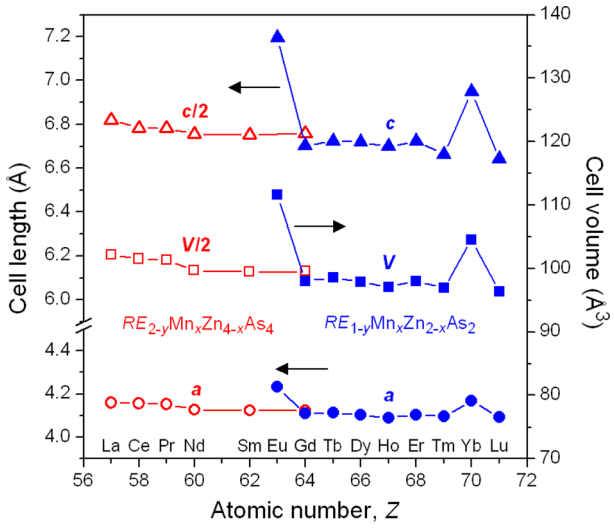

Figure 2. Plots of cell parameters for $REMn_{0.5}Zn_{1.5}As_2$ (*RE* = Eu, Yb), $RE_{0.5}Mn_{0.4}Zn_{1.6}As_2$ (*RE* = Gd−Tm, Lu), and $RE_{1.3}Mn_{0.9}Zn_{3.1}As_4$ (*RE* = La−Nd, Sm, Gd).

The parent $CaAl_2Si_2$-type structure is retained for $REMn_{0.4}Zn_{1.6}As_2$ (*RE* = Eu, Yb), in which a disordered mixture of Mn and Zn atoms occupy the unique transition-metal site, surrounded by As atoms forming M-centered tetrahedra that share their edges to build up $[M_2As_2]$ slabs. These slabs are

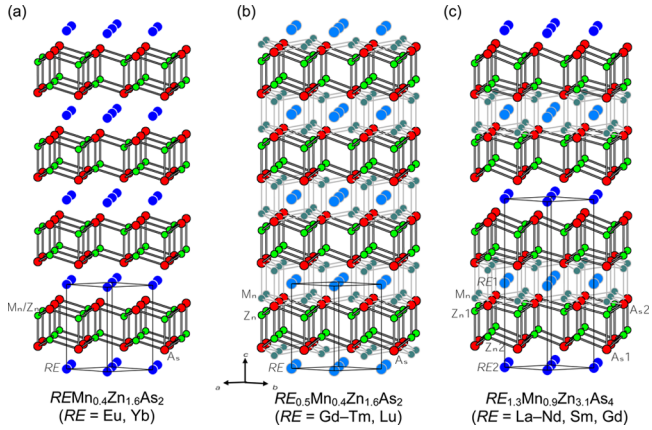

Figure 3. (a) $REMn_{0.4}Zn_{1.6}As_2$ (*RE* = Eu, Yb) with $CaAl_2Si_2$-type structure, (b) $RE_{0.5}Mn_{0.4}Zn_{1.6}As_2$ (*RE* = Gd−Tm, Lu) with defect $CaAl_2Si_2$-type structure, and (c) $RE_{1.3}Mn_{0.9}Zn_{3.1}As_4$ (*RE* = La−Nd, Sm, Gd) with partially ordered defect $CaAl_2Si_2$-type structure; all contain $[M_2As_2]$ slabs alternately stacked with nets of *RE* atoms. The *RE* sites are either fully (dark blue) or partially occupied (faded blue). The interstitial Mn sites are partially occupied (faded blue-green). The Zn sites in (b) and the Zn1 sites in (c) are partially occupied (green).

interleaved with hexagonal nets of fully occupied *RE* sites, each surrounded by As atoms in octahedral geometry (Figure 3a). These quaternary arsenides may be assumed to be members of solid solutions formed between the known parent ternary arsenides $REMn_2As_2$[60] and $REZn_2As_2$ (for *RE* = Eu, Yb).[27,28,45−48] Indeed, for the Eu-containing quaternary compound, the cell parameters (a = 4.234(2) Å, c = 7.198(4) Å) are intermediate between those of $EuMn_2As_2$ (a = 4.287(1) Å, c = 7.225(1) Å)[60] and $EuZn_2As_2$ (a = 4.211(1) Å, c = 7.181(1) Å).[27] If a linear relationship is assumed between cell parameters and concentration (Vegard's law), a composition of 30% Mn and 70% Zn is obtained, in good agreement with the precise composition of $EuMn_{0.5}Zn_{1.5}As_2$ determined in the structure refinement. However, comparison of the cell parameters for the Yb-containing quaternary compound (a = 4.168(1) Å, c = 6.948(1) Å) with those of $YbMn_2As_2$ (a = 4.226(3) Å, c = 6.964(5) Å)[60] and $YbZn_2As_2$ (a = 4.157(1) Å, c = 6.954(1) Å)[48] reveals anomalous behavior. Although the a-parameter is intermediate and suggests a composition of 83% Zn, in agreement with the refined formula $YbMn_{0.3}Zn_{1.7}As_2$, the c-parameter is even lower than for the end-members (i.e., a negative deviation from Vegard's law). Mixed valency of Yb has been proposed in $YbZn_2As_2$, with evidence taken from magnetic measurements.[48] The introduction of smaller Yb^{3+} species, whose concentration could conceivably vary within a solid solution, would then act to contract the unit cell parameters more than expected. Alternatively, there may be subtle effects related to the competition between inequivalent Zn−As vs Mn−As bonds within the tetrahedral sites, as discussed below, that are responsible for this anomaly. Elucidation of the full solid solutions $REMn_xZn_{2-x}As_2$ (*RE* = Eu, Yb) and determination of the crystal structures of additional members will be helpful in clarifying these effects.

The formation of these quaternary arsenides $REMn_{0.4}Zn_{1.6}As_2$ (*RE* = Eu, Yb) also tests an important structural feature of $CaAl_2Si_2$-type phases. Within the M-centered tetrahedra, there is an inequivalence between the three lateral or "rib" bonds and the one vertical or "handle" bond. Both experimental observations and theoretical studies indicate that the three rib bonds are normally shorter than the handle bond for M atoms with d^0

dx.doi.org/10.1021/ic501053v | *Inorg. Chem.* 2014, 53, 8431−8441

(e.g., Mg, Al) and d^{10} configurations (e.g., Zn, Cd),[9] whereas the trend is more muted or even reversed for M atoms with d^5 configurations (e.g., Mn).[2] Although full crystal structures are not available for all the parent ternary arsenides $REMn_2As_2$ and $REZn_2As_2$ (*RE* = Eu, Yb), their bond lengths can be estimated with the assumption of atomic coordinates taken from related $CaAl_2Si_2$-type structures. The distinction predicted for these two types of M−As bonds, depending on the d-configuration of M, is demonstrated clearly in $EuMn_2As_2$ (2.622 Å ribs, 2.601 Å handle) versus $EuZn_2As_2$ (2.549 Å ribs, 2.614 Å handle) (Figure 4), and

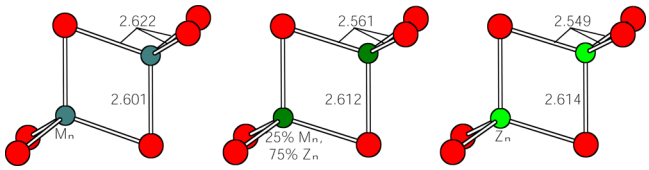

Figure 4. Lengths (Å) of rib and handle bonds within metal-centered tetrahedra in $EuMn_2As_2$ (left), $EuMn_{0.4}Zn_{1.6}As_2$ (center), and $EuZn_2As_2$ (right).

in $YbMn_2As_2$ (2.579 Å ribs, 2.507 Å handle) versus $YbZn_2As_2$ (2.520 Å ribs, 2.595 Å handle). The driving force for this bond inequivalence is the filling of some antibonding states for the handle bonds near the Fermi level, which can be avoided in the d^5 case if a low-spin configuration is adopted.[2,9] In the quaternary arsenides, the larger concentration of Zn atoms and the greater electronic flexibility of Mn atoms together result in the normal situation of shorter rib than handle bonds (i.e., 2.561(2) Å ribs, 2.612(2) Å handle in $EuMn_{0.5}Zn_{1.5}As_2$ (Figure 4); 2.533(1) Å ribs, 2.612(1) Å handle in $YbMn_{0.3}Zn_{1.7}As_2$).

Replacing the divalent *RE* with late trivalent *RE* metals results in the series of quaternary arsenides $RE_{0.5}Mn_{0.4}Zn_{1.6}As_2$ (*RE* = Gd−Tm, Lu) containing deficiencies in the *RE* site as well as a secondary transition-metal site close to the original one. Because refinements suggest a preference of Zn atoms for the primary site and Mn atoms for the secondary site, we have assumed an ordered model. The Zn atoms reside within $[Zn_{1.6}As_2]$ slabs, whereas the Mn atoms partially occupy (∼0.2) interstitial sites located above and below these slabs, in the space made available by the *RE* vacancies (Figure 3b). The Zn-centered tetrahedra within the slabs exhibit shorter rib (2.52−2.53 Å) than handle Zn−As bonds (2.57−2.61 Å), in accordance with expectations; the As−Zn−As angles around the base of these tetrahedra (108.3−108.6°) remain similar to those (110.7−111.5°) in $REMn_{0.4}Zn_{1.6}As_2$ (*RE* = Eu, Yb). The Mn atoms are also surrounded in tetrahedral geometry by three As atoms capping one $[Zn_{1.6}As_2]$ slab and a fourth As atom capping the adjacent $[Zn_{1.6}As_2]$ slab. These Mn-centered tetrahedra are more distorted, with much shorter rib (2.40−2.42 Å) than handle bonds (2.66−2.87 Å) and wider As−Mn−As angles (116.1−117.4°) around the base of these tetrahedra. Perhaps a better description of the Mn coordination is CN3 + 1.

The appearance of *RE* defects in quaternary arsenides $RE_{0.5}Mn_{0.4}Zn_{1.6}As_2$ (*RE* = Gd−Tm, Lu) can be rationalized in the same way as in the previously reported ternary arsenides $RE_{0.67}Zn_2As_2$ (*RE* = La−Nd, Sm),[24] namely, to reduce the number of valence electrons to satisfy charge balance requirements when trivalent *RE* components are introduced. If divalent Mn and Zn atoms are assumed, the ideal charge-balanced formula is $RE_{0.67}Mn_{0.4}Zn_{1.6}As_2$, but the observed *RE* deficiencies are somewhat more pronounced. Note that a slight deviation was also seen in $Ce_{0.63}Zn_2As_2$, the only member of $RE_{0.67}Zn_2As_2$ that has been structurally refined.[24] Alternatively, the formula $RE_{0.5}Mn_{0.4}Zn_{1.6}As_2$ would be almost perfectly charge-balanced if Mn^{3+} species are assumed instead. In any event, these chemical formulas should be accepted cautiously because structural refinements of occupancies may be correlated with other factors (such as absorption corrections). Moreover, as mentioned in the introduction, exceptions to the ideal electron count are permissible when there is no band gap at the Fermi level, a notion to be tested by a band structure calculation discussed further below. As in $RE_{0.67}Zn_2As_2$ (*RE* = La−Nd, Sm), no vacancy ordering was apparent in $RE_{0.5}Mn_{0.4}Zn_{1.6}As_2$ (*RE* = Gd−Tm, Lu), as evaluated by the absence of superstructure reflections or diffuse scattering in the X-ray diffraction patterns (Figure S1 in Supporting Information and Figure 1). In the related ternary sulfides $RE_{0.67}Cu_2S_2$, which also adopt defect $CaAl_2Si_2$-type structures, there is evidence that short-range ordering may take place.[61,62] Various stacking sequences can be envisioned for the hexagonal *RE* nets, each containing an ordered distribution of 33% vacancies (and 67% occupied sites), such that proximity of *RE* vacancies in adjacent nets is avoided. Long-range ordering within these sequences is frustrated by the occurrence of frequent stacking faults. The situation in $RE_{0.5}Mn_{0.4}Zn_{1.6}As_2$ (*RE* = Gd−Tm, Lu) is complicated by the occurrence of vacancies not only in the *RE* sites, but also in the Mn and Zn sites.

It is thus remarkable that partial long-range ordering does occur, in a different manner than described above, through substitution with the early trivalent *RE* metals in the series $RE_{1.3}Mn_{0.9}Zn_{3.1}As_4$ (*RE* = La−Nd, Sm, Gd). The formula is nearly twice that of $RE_{0.5}Mn_{0.4}Zn_{1.6}As_2$, reflecting a doubling of the *c*-parameter. In this superstructure, hexagonal nets of completely filled *RE*2 sites alternately stack with nets of partially filled (∼0.3) *RE*1 sites (Figure 3c). Within the $[Zn_{1.6}As_2]$ slabs, there is now a differentiation between fully occupied Zn2 sites adjacent to the filled *RE*2 nets and partially occupied (∼0.6) Zn1 sites adjacent to the defective *RE*1 nets. As before, the Mn atoms reside in interstitial sites within the defective layers. Curiously, although the Zn1-centered tetrahedra retain the expected distinction of bonds to the surrounding As atoms (shorter ribs, 2.47−2.50 Å; longer handle, 2.72−2.78 Å), the Zn2-centered tetrahedra show a reversal (longer ribs, 2.56−2.57 Å; shorter handle, 2.49−2.52 Å). Although the structure refinements do indicate clear site preferences for the Mn and Zn atoms, partial disorder cannot be completely ruled out, which may account for this bond length reversal. We think that the combination of substitutional and positional disorder (Mn vs Zn) and the presence of *RE* defects present many competing size and electronic factors that complicate the structural analysis. For example, an alternative explanation for the rather short Zn1−As2 and Mn−As2 distances of ∼2.5 Å is that they compensate for the "underbonding" of the As2 atoms next to vacant *RE*1 sites. Moreover, there is growing recognition that in AB_2X_2 compounds with the $CaAl_2Si_2$-type structure, the *A* cations may participate in covalent interactions with the $[B_2X_2]$ slabs, notwithstanding earlier assumptions that their role was not significant.[14] The contrast between the partially ordered series $RE_{1.3}Mn_{0.9}Zn_{3.1}As_4$ (formed for the earlier *RE* metals) and the disordered series $RE_{0.5}Mn_{0.4}Zn_{1.6}As_2$ (formed for the later *RE* metals) suggests that such interactions may indeed be important. Note that the *RE*1−As2 distances straddling the interstitial Mn sites are nearly invariant (2.86−2.88 Å), whereas the *RE*2−As1 distances decrease gradually (from 3.01 Å in the La member to 2.92 Å in the Gd member); these observations

dx.doi.org/10.1021/ic501053v | Inorg. Chem. 2014, 53, 8431−8441

suggest that Mn−As bonds dictate the spacing between one pair of $[Zn_{1.6}As_2]$ slabs, while *RE*−As bonds are optimal between the other pair of $[Zn_{1.6}As_2]$ slabs.

With slightly different loading compositions used in the syntheses of the Gd-containing compounds, members belonging to both series, $Gd_{0.5}Mn_{0.4}Zn_{1.6}As_2$ and $Gd_{1.2}Mn_{0.9}Zn_{3.1}As_4$, could be obtained. In principle, vacancy ordering could be promoted through use of extended annealing times and slow cooling. Although these procedures do improve crystal quality (as gauged by sharpness of X-ray diffraction peaks), they did not alleviate the disorder even in the $Gd_{1.2}Mn_{0.9}Zn_{3.1}As_4$ superstructure. We investigated the possibility for the existence of a solid solution through preliminary experiments with loading compositions $Gd_{0.67}Mn_xZn_{2-x}As_2$ (for x = 0, 0.05, 0.1, 0.3, 0.5, 1.0, 1.5, 2.0) adhering to the ideal electron count. The products were not single-phase and contained admixtures of various binary arsenides, probably because of problems with volatilization described earlier. It appears that $CaAl_2Si_2$-type phases can be formed up to a Mn loading composition of x = 1.0 (i.e., 50% Mn), and evidence for superstructure peaks occurs for loading compositions of x = 0.3−1.0 (i.e., 15−50% Mn) (Figure S4 in Supporting Information); the true compositions undoubtedly contain lower Mn concentrations. The ternary end-member $Gd_{0.67}Mn_2As_2$ did not form. In addition to the disorder of Mn and Zn atoms, there is also the possibility for a homogeneity range in the Gd content, which will require future investigations on $Gd_{1-y}Mn_xZn_{2-x}As_2$ to probe the extent of Gd deficiencies (y).

The partial substitution of Mn (d^5) for Zn (d^{10}) presents an interesting scenario for the electronic structure. A small band gap is expected for most AB_2X_2 phases with the $CaAl_2Si_2$-type structure when the B component has a d^{10} (or d^0) configuration. However, the Fermi level will necessarily cross a d-band when the B component has a d^5 configuration, as previously shown for a $[Mn_2P_2]^{2-}$ slab.[2] Taking the idealized formula as $La_{1.33}MnZn_3As_4$, which would be electron-precise if divalent Mn and Zn atoms are assumed, we can propose a $\sqrt{3}a \times \sqrt{3}a$ superstructure (Figure 5). The La1 nets contain an ordered

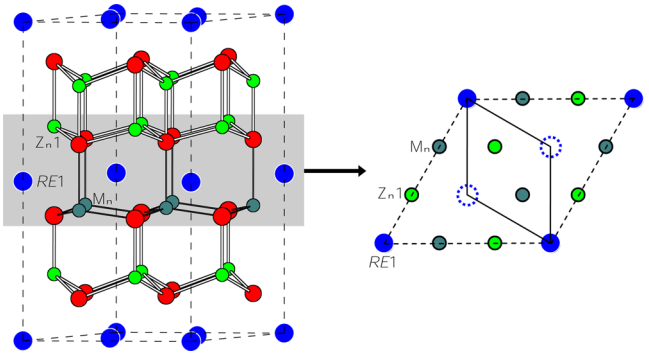

Figure 5. Possible $\sqrt{3}a \times \sqrt{3}a$ superstructure (with unit cell outlined in dashed lines) for idealized model $La_{1.33}MnZn_3As_4$ containing ordered occupation of 33% La, 50% Mn, and 50% Zn1 sites.

distribution of the 33% filled sites. The Mn and Zn1 sites, each 50% occupied, are within ~1.0 Å of each other and cannot be simultaneously occupied within the same slab (Figure 3c). Instead, we imagine that they segregate into $[MnZnAs_2]$ and $[Zn_2As_2]$ slabs, with long 2.8 Å Mn−As bonds connecting them. The density of states (DOS) curve for this hypothetical superstructure was determined from band structure calculations (Figure 6a). The features of the DOS curve are generally

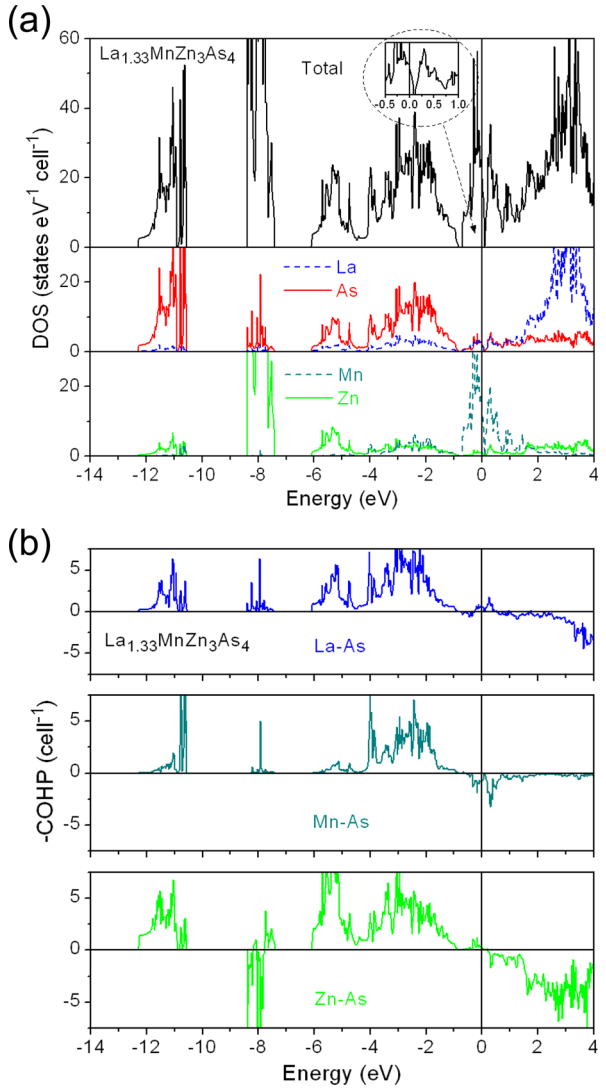

Figure 6. (a) Density of states (DOS) and its atomic projections for $La_{1.33}MnZn_3As_4$. (b) Crystal orbital Hamilton population (COHP) curves for La−As, Mn−As, and Zn−As interactions. The Fermi level is at 0 eV.

consistent with the formulation $(La^{3+})_{1.33}(Mn^{2+})(Zn^{2+})_3(As^{3-})_4$ derived from the Zintl concept in which the electropositive La atoms fully transfer their valence electrons to the anionic slabs. Thus, empty La-based states are mostly found above the Fermi level, and filled As 4s and 4p states are found below. The Zn 3d states are completely filled (−8 eV), whereas the Mn 3d states are partially filled (−1 to +1 eV). Most of the bonding stability comes from the occupation of Mn−As and Zn−As bonding levels, derived from significant mixing of Mn 3d or Zn 3d with As 4s/4p states, but there are also important covalent contributions to La−As bonding, as seen in the crystal orbital Hamilton population (COHP) curves (Figure 6b). The integrated COHP values (−ICOHP) are 2.4 eV/bond for Mn−As, 1.7 eV/bond for Zn−As, and 1.0 eV/bond for La−As interactions. Note that the states near the Fermi level are antibonding for the Mn−As interactions, but only weakly bonding for the Zn−As and La−As interactions. Thus, the possibility exists to alleviate the antibonding Mn−As interactions by reducing the electron count to lower the Fermi level slightly. This partial oxidation could be manifested experimentally through

dx.doi.org/10.1021/ic501053v | Inorg. Chem. 2014, 53, 8431−8441

greater La or Mn deficiencies, as suggested by the formula $La_{1.2}Mn_{0.9}Zn_{3.1}As_4$ refined in the structure determination, or by invoking the presence of some Mn^{3+} species. Low-spin Mn is implicit in the filling of the d-band near the Fermi level, but the conclusions are unchanged if high-spin Mn is assumed, for which there would be an even greater driving force to reduce the electron count.

The large spike in the DOS near the Fermi level is derived from mostly Mn 3d states and suggests an electronic instability. In a spin-polarized calculation of $La_{1.33}MnZn_3As_4$, the DOS curve reveals that such a high polarization is indeed predicted (Figure 7), with a large energy stabilization of 2.6 eV/cell. The

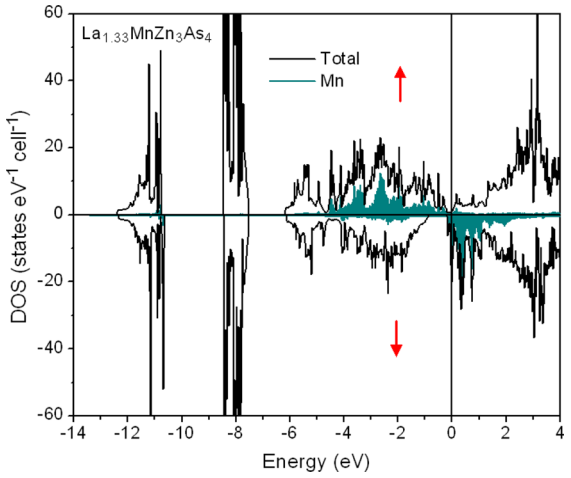

Figure 7. DOS curve for spin-polarized $La_{1.33}MnZn_3As_4$, with contributions from Mn states identified by the shaded regions.

magnetic moment is calculated to be 3.6 μ_B. This compound is nearly a ferromagnetic half-metal: for the spin-up electrons, the Fermi level falls in a pseudogap with almost zero DOS, whereas for the spin-down electrons, it intersects the bottom of the conduction band.

To acquire experimental evidence for the valence state assignments, XPS spectra were collected for $YbMn_{0.3}Zn_{1.7}As_2$, $Er_{0.5}Mn_{0.4}Zn_{1.6}As_2$, and $Nd_{1.2}Mn_{1.0}Zn_{3.0}As_4$ as representative members of the different series of quaternary arsenides. Among the *RE* components, only the Yb valence is really subject to question. The Yb 4d spectrum for $YbMn_{0.3}Zn_{1.7}As_2$, obtained after a sputtering procedure was applied to eliminate surface oxides, reveals the presence of both Yb^{2+} and Yb^{3+} (Figure 8a). The Yb $4d_{5/2}$ core-line peak at 184.9 eV is identical to that in Yb_2O_3, measured as a Yb^{3+}-containing standard. Many of the undulations in the fine structure for $YbMn_{0.3}Zn_{1.7}As_2$ are also found in Yb_2O_3, with the exception of a prominent low-energy shoulder at 181.3 eV that is consistent with the 4d core-line peak for Yb^{2+}.[63] In a similar XPS study on the related antimonide $YbZn_2Sb_2$, both Yb^{2+} and Yb^{3+} were also found to be present, but it was suggested that formation of Yb_2O_3 within grain boundaries is likely responsible for the residual Yb^{3+} signature.[19] Given this caveat, the occurrence of mixed-valent Yb in $YbMn_{0.3}Zn_{1.7}As_2$ remains inconclusive.

The formal assignments of Zn^{2+} and As^{3-} are hardly disputable, but it is unclear if Mn^{2+} is exclusively present in all cases. The Mn 2p spectra for $YbMn_{0.3}Zn_{1.7}As_2$, $Er_{0.5}Mn_{0.4}Zn_{1.6}As_2$, and $Nd_{1.2}Mn_{1.0}Zn_{3.0}As_4$ confirm that Mn^{2+} is indeed the dominant species present (Figure 8b). The spectra can be resolved into three component peaks (A–C), consistent with

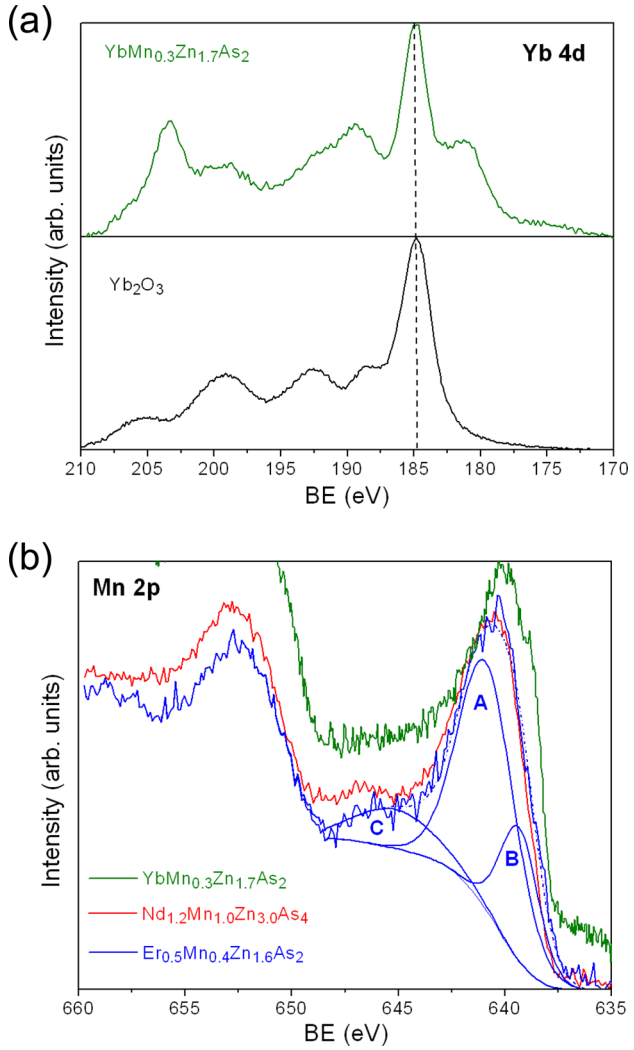

Figure 8. (a) Yb 4d XPS spectra for $YbMn_{0.3}Zn_{1.7}As_2$ and Yb_2O_3. (b) Mn 2p XPS spectra for $YbMn_{0.3}Zn_{1.7}As_2$, $Nd_{1.2}Mn_{1.0}Zn_{3.0}As_4$, and $Er_{0.5}Mn_{0.4}Zn_{1.6}As_2$. The components marked A–C are discussed in the text.

other Mn^{2+}-containing compounds.[64,65] Peak A, the main Mn $2p_{3/2}$ core-line peak, occurs at 640.1 eV for $YbMn_{0.3}Zn_{1.7}As_2$, 641.0 eV for $Nd_{1.2}Mn_{1.0}Zn_{3.0}As_4$, and 640.9 eV for $Er_{0.5}Mn_{0.4}Zn_{1.6}As_2$. These binding energies (BE) are higher than they are in elemental Mn (639.7(8) eV), within the ranges exhibited by various Mn^{2+}-containing compounds (MnS, 640.5–642.1 eV; MnO, 641.2(5) eV; (Ga,Mn)As, 641.0 eV), and lower than they are in Mn^{3+}-containing compounds (Mn_2O_3, 641.6(2) eV).[66−72] The BE of 640.1 eV in $YbMn_{0.3}Zn_{1.7}As_2$ is noticeably shifted relative to the others (as seen in the spectrum, offset vertically for clarity, in Figure 8b), but we attribute this observation to a slight reduction caused by Ar^+ sputtering procedure, which had to be performed for a longer time to improve the poor signal quality in this sample containing low Mn concentrations. Peak B is located to slightly lower BE from the core-line peak; this shoulder results from the Ar^+ sputtering procedure and is commonly found in Mn^{2+} systems.[64,65] Peak C is an important diagnostic feature: it is a metal-to-ligand shakeup satellite peak that occurs only for Mn^{2+} and is absent for Mn^{3+} and Mn^{4+}.[72−76] It is found at 645.8 eV for $Nd_{1.2}Mn_{1.0}Zn_{3.0}As_4$ and 645.2 eV for $Er_{0.5}Mn_{0.4}Zn_{1.6}As_2$, but is difficult to locate for $YbMn_{0.3}Zn_{1.7}As_2$ probably because it was

dx.doi.org/10.1021/ic501053v | Inorg. Chem. 2014, 53, 8431−8441

weakened in relative intensity through the increased sputtering time until it became buried beneath the background. The XPS results do strongly imply that Mn^{2+} is present in these compounds.

CONCLUSIONS

Many subtle factors are at play in the partial substitution of Mn for Zn in these rare-earth zinc arsenides with the $CaAl_2Si_2$-type structure. In the simplest case involving the divalent *RE* components, the compounds $REMn_{0.4}Zn_{1.6}As_2$ (*RE* = Eu, Yb) keep the parent structure; the Mn and Zn atoms disorder within the same tetrahedral site, and the distinction between rib and handle bonds in this site is controlled by the Zn atoms. In the more complex cases involving the trivalent *RE* components, the vacancies introduced into the hexagonal nets permit Mn atoms to occupy alternative tetrahedral sites close to the original Zn sites. For $RE_{0.5}Mn_{0.4}Zn_{1.6}As_2$ (*RE* = Gd−Tm, Lu), considerable disorder ensues from the occurrence of *RE* vacancies, probably in the form of stacking faults of the hexagonal *RE* nets, as well as from the split Mn/Zn sites. For $RE_{1.3}Mn_{0.9}Zn_{3.1}As_4$ (*RE* = La−Nd, Sm, Gd), the disorder is partially resolved through the segregation of completely filled *RE* nets and 33% occupied *RE* nets. The distinction between these two series, for the early versus late trivalent *RE* members, supports the proposal that the *A*-cation in AB_2X_2 phases with the $CaAl_2Si_2$-type structure does participate in bonding with the $[B_2X_2]$ slabs and can thus indirectly influence electronic properties. Given the relatively high concentration of Mn in these quaternary arsenides, the electronic structure is dominated by a partially filled Mn-based d-band near the Fermi level, as shown for $La_{1.33}MnZn_3As_4$, so that metallic behavior is predicted. We believe that Mn can likely be introduced at lower concentrations while a band gap is retained, so that the resulting compounds may be good candidates as magnetic semiconductors. Attempts to prepare Gd-containing solid solutions suggest that the Mn concentration can indeed be varied, but further efforts are required to optimize phase purity before magnetic measurements can be performed.

ASSOCIATED CONTENT

Supporting Information

X-ray crystallographic files in CIF format, powder XRD patterns, and EDX analyses. This material is available free of charge via the Internet at http://pubs.acs.org. Additional CIF files may be obtained from Fachinformationszentrum Karlsruhe, Abt. PROKA, 76344 Eggenstein-Leopoldshafen, Germany (No. CSD-427692 to 427706).

AUTHOR INFORMATION

Corresponding Author

*E-mail: arthur.mar@ualberta.ca.

Notes

The authors declare no competing financial interest.

ACKNOWLEDGMENTS

This work was supported by the Natural Sciences and Engineering Research Council of Canada.

REFERENCES

(1) Hoffmann, R.; Zheng, C. *J. Phys. Chem.* **1985**, *89*, 4175−4181.
(2) Zheng, C.; Hoffmann, R. *J. Solid State Chem.* **1988**, *72*, 58−71.
(3) Johrendt, D.; Felser, C.; Jepsen, O.; Andersen, O. K.; Mewis, A.; Rouxel, J. *J. Solid State Chem.* **1997**, *130*, 254−265.
(4) Rotter, M.; Pangerl, M.; Tegel, M.; Johrendt, D. *Angew. Chem., Int. Ed.* **2008**, *47*, 7949−7952.
(5) Johrendt, D.; Pöttgen, R. *Physica C* **2009**, *469*, 332−339.
(6) Mandrus, D.; Sefat, A. S.; McGuire, M. A.; Sales, B. C. *Chem. Mater.* **2010**, *22*, 715−723.
(7) Paglione, J.; Greene, R. L. *Nat. Phys.* **2010**, *6*, 645−658.
(8) Klüfers, P.; Mewis, A. *Z. Kristallogr.* **1984**, *169*, 135−147.
(9) Zheng, C.; Hoffmann, R.; Nesper, R.; von Schnering, H.-G. *J. Am. Chem. Soc.* **1986**, *108*, 1876−1884.
(10) Burdett, J. K.; Miller, G. J. *Chem. Mater.* **1990**, *2*, 12−26.
(11) Kranenberg, C.; Johrendt, D.; Mewis, A. *Z. Anorg. Allg. Chem.* **1999**, *625*, 1787−1793.
(12) Kranenberg, C.; Johrendt, D.; Mewis, A. *Solid State Sci.* **2002**, *4*, 261−265.
(13) Wartenberg, F.; Kranenberg, C.; Pocha, R.; Johrendt, D.; Mewis, A.; Hoffmann, R.-D.; Mosel, B. D.; Pöttgen, R. *Z. Naturforsch., B: Chem. Sci.* **2002**, *57*, 1270−1276.
(14) Alemany, P.; Llunell, M.; Canadell, E. *J. Comput. Chem.* **2008**, *29*, 2144−2153.
(15) Kauzlarich, S. M.; Brown, S. R.; Snyder, G. J. *Dalton Trans.* **2007**, 2099−2107.
(16) Toberer, E. S.; May, A. F.; Snyder, G. J. *Chem. Mater.* **2010**, *22*, 624−634.
(17) Zhang, H.; Zhao, J.-T.; Grin, Yu.; Wang, X.-J.; Tang, M.-B.; Man, Z.-Y.; Chen, H.-H.; Yang, X.-X. *J. Chem. Phys.* **2008**, *129*, 164713−1−164713−5.
(18) Zhang, H.; Fang, L.; Tang, M.-B.; Chen, H.-H.; Yang, X.-X.; Guo, X.; Zhao, J.-T.; Grin, Yu. *Intermetallics* **2010**, *18*, 193−198.
(19) Flage-Larsen, E.; Diplas, S.; Prytz, Ø.; Toberer, E. S.; May, A. F. *Phys. Rev. B* **2010**, *81*, 205204−1−205204−7.
(20) May, A. F.; McGuire, M. A.; Singh, D. J.; Ma, J.; Delaire, O.; Huq, A.; Cai, W.; Wang, H. *Phys. Rev. B* **2012**, *85*, 035202−1−035202−10.
(21) Pomrehn, G. S.; Zevalkink, A.; Zeier, W. G.; van de Walle, A.; Snyder, G. J. *Angew. Chem., Int. Ed.* **2014**, *53*, 3422−3426.
(22) Gascoin, F.; Ottensmann, S.; Stark, D.; Haïle, S. M.; Snyder, G. J. *Adv. Funct. Mater.* **2005**, *15*, 1860−1864.
(23) Villars, P.; Cenzual, K. *Pearson's Crystal Data—Crystal Structure Database for Inorganic Compounds;* ASM International: Materials Park, OH, 2010.
(24) Nientiedt, A. T.; Lincke, H.; Rodewald, U. Ch.; Pöttgen, R.; Jeitschko, W. *Z. Naturforsch., B: Chem. Sci.* **2011**, *66*, 221−226.
(25) Klüfers, P.; Mewis, A.; Schuster, H.-U. *Z. Kristallogr.* **1979**, *149*, 211−225.
(26) Mewis, A. *Z. Naturforsch., B: Anorg. Chem., Org. Chem.* **1980**, *35*, 939−941.
(27) Klüfers, P.; Neumann, H.; Mewis, A.; Schuster, H.-U. *Z. Naturforsch., B: Anorg. Chem., Org. Chem.* **1980**, *35*, 1317−1318.
(28) Zwiener, G.; Neumann, H.; Schuster, H.-U. *Z. Naturforsch., B: Anorg. Chem., Org. Chem.* **1981**, *36*, 1195−1197.
(29) Mahan, A.; Mewis, A. *Z. Naturforsch., B: Anorg. Chem., Org. Chem.* **1983**, *38*, 1041−1045.
(30) Tejedor, P.; Stacy, A. M. *J. Solid State Chem.* **1990**, *89*, 227−236.
(31) Blanchard, P. E. R.; Stoyko, S. S.; Cavell, R. G.; Mar, A. *J. Solid State Chem.* **2011**, *184*, 97−103.
(32) Nateprov, A. N.; Kravtsov, V. Ch.; Moshnyaga, V.; Schorr, S. *Elektron. Obrab. Mater.* **2012**, *48*, 94−98.
(33) Stoyko, S. S.; Ramachandran, K. K.; Blanchard, P. E. R.; Rosmus, K. A.; Aitken, J. A.; Mar, A. *J. Solid State Chem.* **2014**, *213*, 275−286.
(34) Ponnambalam, V.; Lindsey, S.; Xie, W.; Thompson, D.; Drymiotis, F.; Tritt, T. M. *J. Phys. D: Appl. Phys.* **2011**, *44*, 155406−1−155406−6.
(35) Ponnambalam, V.; Morelli, D. T. *J. Electron. Mater.* **2014**, *43*, 1875−1880.
(36) Yu, C.; Zhu, T. J.; Zhang, S. N.; Zhao, X. B.; He, J.; Su, Z.; Tritt, T. M. *J. Appl. Phys.* **2008**, *104*, 013705−1−013705−5.

(37) Wang, X.-J.; Tang, M.-B.; Chen, H.-H.; Yang, X.-X.; Zhao, J.-T.; Burkhardt, U.; Grin, Yu. *Appl. Phys. Lett.* **2009**, *94*, 092106−1−092106−3.
(38) Zhang, H.; Baitinger, M.; Tang, M.-B.; Man, Z.-Y.; Chen, H.-H.; Yang, X.-X.; Liu, Y.; Chen, L.; Grin, Yu.; Zhao, J.-T. *Dalton Trans.* **2010**, *39*, 1101−1104.
(39) Cao, Q.-G.; Zhang, H.; Tang, M.-B.; Chen, H.-H.; Yang, X.-X.; Grin, Yu.; Zhao, J.-T. *J. Appl. Phys.* **2010**, *107*, 053714−1−053714−5.
(40) Zhang, H.; Fang, L.; Tang, M.-B.; Man, Z.-Y.; Chen, H.-H.; Yang, X.-X.; Baitinger, M.; Grin, Yu.; Zhao, J.-T. *J. Chem. Phys.* **2010**, *133*, 194701−1−194701−5.
(41) Guo, K.; Cao, Q.-G.; Feng, X.-J.; Tang, M.-B.; Chen, H.-H.; Guo, X.; Chen, L.; Grin, Yu.; Zhao, J.-T. *Eur. J. Inorg. Chem.* **2011**, 4043−4048.
(42) Zhao, L.-D.; Lo, S.-H.; Zhang, Y.; Sun, H.; Tan, G.; Uher, C.; Wolverton, C.; Dravid, V. P.; Kanatzidis, M. G. *Nature* **2014**, *508*, 373−377.
(43) Deng, Z.; Jin, C. Q.; Liu, Q. Q.; Wang, X. C.; Zhu, J. L.; Feng, S. M.; Chen, L. C.; Yu, R. C.; Arguello, C.; Goko, T.; Ning, F.; Zhang, J.; Wang, Y.; Aczel, A. A.; Munsie, T.; Williams, T. J.; Luke, G. M.; Kakeshita, T.; Uchida, S.; Higemoto, W.; Ito, T. U.; Gu, B.; Maekawa, S.; Morris, G. D.; Uemura, Y. J. *Nat. Commun.* **2011**, *2*, 422−1−422−5.
(44) Deng, Z.; Zhao, K.; Gu, B.; Han, W.; Zhu, J. L.; Wang, X. C.; Li, X.; Liu, Q. Q.; Yu, R. C.; Goko, T.; Frandsen, B.; Liu, L.; Zhang, J.; Wang, Y.; Ning, F. L.; Maekawa, S.; Uemura, Y. J.; Jin, C. Q. *Phys. Rev. B* **2013**, *88*, 081203−1−081203−5.
(45) Altshuler, T. S.; Goryunov, Yu. V.; Nateprov, A. V. *J. Phys.: Conf. Ser.* **2011**, *324*, 012020−1−012020−5.
(46) Goryunov, Yu.; Fritsch, V.; von Löhneysen, H.; Nateprov, A. *J. Phys.: Conf. Ser.* **2012**, *391*, 012015−1−012015−4.
(47) Goryunov, Yu. V.; Levchenko, A. V.; Nateprov, A. N. *J. Phys.: Conf. Ser.* **2012**, *400*, 032013−1−032013−4.
(48) Nateprov, A.; Cisowski, J.; Heimann, J.; Mirebeau, I. *J. Alloys Compd.* **1999**, *290*, 6−9.
(49) Lin, X.; Stoyko, S. S.; Mar, A. *J. Solid State Chem.* **2013**, *199*, 189−195.
(50) Stoyko, S. S.; Mar, A. *J. Solid State Chem.* **2011**, *184*, 2360−2367.
(51) Stoyko, S. S.; Mar, A. *Inorg. Chem.* **2011**, *50*, 11152−11161.
(52) Lin, X.; Mar, A. *Inorg. Chem.* **2013**, *52*, 7261−7270.
(53) Stoyko, S. S.; Khatun, M.; Mar, A. *Inorg. Chem.* **2012**, *51*, 2621−2628.
(54) Saparov, B.; Bobev, S. *Acta Crystallogr., Sect. E: Struct. Rep. Online* **2010**, *66*, i24.
(55) Sheldrick, G. M. *SHELXTL,* version 6.12; Bruker AXS Inc.: Madison, WI, 2001.
(56) Gladyshevskii, E. I.; Kripyakevich, P. I.; Bodak, O. I. *Ukr. Fiz. Zh.* **1967**, *12*, 447−452.
(57) Gelato, L. M.; Parthé, E. *J. Appl. Crystallogr.* **1987**, *20*, 139−143.
(58) Tank, R.; Jepsen, O.; Burkhardt, A.; Andersen, O. K. *TB-LMTO-ASA Program,* version 4.7; Max Planck Institut für Festkörperforschung: Stuttgart, Germany, 1998.
(59) Fairley, N. *CasaXPS,* version 2.3.9; Casa Software Ltd.: Teighnmouth, Devon, UK, 2003, http://www.casaxps.com.
(60) Rühl, R.; Jeitschko, W. *Mater. Res. Bull.* **1979**, *14*, 513−517.
(61) Guymont, M.; Tomas, A.; Julien-Pouzol, M.; Jaulmes, S.; Guittard, M. *Phys. Status Solidi A* **1990**, *121*, 21−28.
(62) Onoda, M.; Chen, X.; Sato, A.; Wada, H. *J. Solid State Chem.* **2000**, *152*, 332−339.
(63) Suga, S.; Ogawa, S.; Namatame, H.; Taniguchi, M.; Kakizaki, A.; Ishii, T.; Fujimori, A.; Oh, S.-J.; Kato, H.; Miyahara, T.; Ochiai, A.; Suzuki, T.; Kasuya, T. *J. Phys. Soc. Jpn.* **1989**, *58*, 4534−4543.
(64) Iwanowski, R. J.; Heinonen, M. H.; Janik, E. *Chem. Phys. Lett.* **2004**, *387*, 110−115.
(65) Iwanowski, R. J.; Heinonen, M. H.; Janik, E. *Appl. Surf. Sci.* **2005**, *249*, 222−230.
(66) Wagner, C. D.; Naumkin, A. V.; Kraut-Vass, A.; Allison, J. W.; Powell, C. J.; Rumble, J. R., Jr. *NIST X-ray Photoelectron Spectroscopy Database,* version 3.5 (web version); National Institute of Standards and Technology: Gaithersburg, MD, 2003. http://srdata.nist.gov/xps.
(67) Carver, J. C.; Schweitzer, G. K.; Carlson, T. A. *J. Chem. Phys.* **1972**, *57*, 973−982.
(68) Aoki, A. *Jpn. J. Appl. Phys.* **1976**, *15*, 305−311.
(69) Franzen, H. F.; Umaña, M. X.; McCreary, J. R.; Thorn, R. J. *J. Solid State Chem.* **1976**, *18*, 363−368.
(70) Franzen, H. F.; Sterner, C. *J. Solid State Chem.* **1978**, *25*, 227−230.
(71) Di Castro, V.; Polzonetti, G. *J. Electron Spectrosc. Relat. Phenom.* **1989**, *48*, 117−123.
(72) Eid, K. F.; Stone, M. B.; Maksimov, O.; Shih, T. C.; Ku, K. C.; Fadgen, W.; Palstrøm, C. J.; Schiffer, P.; Samarth, N. *J. Appl. Phys.* **2005**, *97*, 10D304−1−10D304−6.
(73) Brisk, M. A.; Baker, A. D. *J. Electron. Spectrosc. Relat. Phenom.* **1975**, *7*, 197−213.
(74) Jeng, S.-P.; Lad, R. J.; Heinrich, V. E. *Phys. Rev. B* **1991**, *43*, 11971−11977.
(75) Stranick, M. A. *Surf. Sci. Spectra* **1999**, *6*, 31−38.
(76) Stranick, M. A. *Surf. Sci. Spectra* **1999**, *6*, 39−46.